This is an open access article published under an ACS AuthorChoice License, which permits copying and redistribution of the article or any adaptations for non-commercial purposes.

ACS OMEGA

Article

Cite This: ACS Omega 2019, 4, 22274−22279

http://pubs.acs.org/journal/acsodf

Electrostrictive Cavitation in Water Induced by a SnO_2 Nanoparticle

Shane Jackson,*[,†,‡] Aiichiro Nakano,*[,†,‡,¶,§] Priya Vashishta,*[,†,‡,¶,§] and Rajiv K. Kalia*[,†,‡,¶,§]

[†]Collaboratory for Advanced Computing and Simulations, [‡]Department of Physics & Astronomy, [¶]Department of Computer Science, and [§]Department of Chemical Engineering & Materials Science, University of Southern California, Los Angeles, California 90089-0242, United States

Supporting Information

ABSTRACT: Cavitation phenomenon in dielectric fluids has been a recent topic of interest in theory and experiment. We study a dielectric fluid−nanoparticle system subjected to an external electric field using molecular dynamics simulations. Electric fields ranging from 0.042 to 0.25 V/Å are applied to a water and tin dioxide system. Cavitation is observed in simulations with both SPC/E water and the hydrogen bonding polarizable model. The cavitation onset time displays a stretched exponential relaxation response with respect to the applied electric field with an exponent $\beta = 0.423 \pm 0.08$. This is in accordance with the exact theoretical value for systems with long-ranged forces. Cavity growth rates are divided into two phases, a spherical growth phase and a cylindrical one. Both are reported as a function of the applied electric field. The structure of the electric field is analyzed both spatially and temporally.

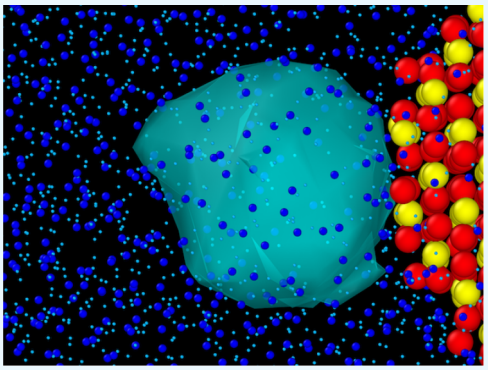

INTRODUCTION

The formation and use of cavities within fluids are rich areas of research and practical applications. Nanobubbles have been used for water treatment, aiding fermentation, and targeted delivery of pharmaceuticals.[1,2] The water jets formed from collapsing nanobubbles can cause structural damage and erosion to important components and, more productively, aid in manufacturing materials.[3] Bubble collapse-induced sonoluminescence has been observed.[4] Typically, cavities arise in the form of gaseous bubbles; however, in this paper, the formation of cavities due to electrostrictive forces will be discussed.

Cavity formation due to negative pressure in water has been the subject of experimental and theoretical work.[5,6] According to the classic nucleation theory, the energy required to generate a spherical void of radius R in a fluid with surface tension σ and pressure P is equal to[7]

$$\Sigma(R) = \frac{4}{3}\pi R^3 P + 4\pi R^2 \sigma \tag{1}$$

The term for the cavity's internal vapor pressure has been excluded as the cavities discussed in this paper have a negligible vapor pressure compared to the internal fluid pressure. Equation 1 implies, for negative pressures, the existence of a critical radius above which it will be energetically favorable for the cavity to continue to grow. Negative pressure can be induced in water (or any dielectric fluid) through the application of a spatially inhomogeneous external applied electric field. This induced negative pressure in a dielectric fluid is given by

$$P = -\frac{1}{2}\alpha\epsilon\epsilon_0 E^2 \tag{2}$$

where ϵ_0 is the vacuum permittivity, ϵ is the dielectric constant of the liquid media, E is the applied electric field, and α is a constant that ranges between 1.3 and 1.5 for most polar liquids.[8] Negative pressure in water has been measured through the Berthelot method with pressures ranging from −3.4 to −12 MPa across temperatures ranging from 275 to 300 K; however, the accuracy of these results has been questioned.[9] Negative pressures exceeding −100 MPa were achieved using water inclusions in quartz;[10] however, in the studies done by Green et al.,[11] each inclusion was only studied a few times or even only once. A better understanding of a cavity formation statistics was provided by Azouzi et al.[5] in which a single inclusion was studied repeatedly. Direct observation of cavities through Rayleigh scattering has been proposed, but to date, no experiments have been carried out.[12] The Shneider, Pekker, and Fridman theory of void formation has been experimentally verified.[12] Water subjected to pulses with rise times of 600 ps to 3 ns were found to generate nanocavities through electrostrictive forces.[13] Cavitation did not occur with longer rise times as the liquid had sufficient time to respond to the forces without rupturing. The theoretical explanation of cavity formation in the presence of a strong, inhomogeneous electric field is found in the work of Shneider and Pekker.[6]

The previous theoretical work cited above has shown the genesis of cavities when a spatially inhomogeneous external field is applied; however, through molecular dynamic simulations, we have witnessed the formation of cavities in water subjected to a spatially constant applied electric field. Inhomogeneities in the

Received: April 5, 2019
Accepted: November 27, 2019
Published: December 18, 2019

Downloaded via UNIV OF SOUTHERN CALIFORNIA on February 26, 2020 at 22:42:39 (UTC).
See https://pubs.acs.org/sharingguidelines for options on how to legitimately share published articles.

© 2019 American Chemical Society

DOI: 10.1021/acsomega.9b00979
ACS Omega 2019, 4, 22274−22279

local electric field occur due to the presence of the tin dioxide nanoparticle. This phenomenon, in turn, leads to void cavitation formation. Simulations of a 1.5 nm SnO_2 nanoparticle immersed in water were performed using LAMMPS (https://lammps.sandia.gov/index.html).[14−16] Electric fields ranging from 0.042 to 0.25 V/Å were applied along the x axis. While the simulated electric field strengths are quite high, water has been experimentally subjected to electric fields between 0.1 and 0.5 V/Å using electrode tips on the order of hundreds of nanometers.[17]

RESULTS AND DISCUSSION

The local electric field was calculated at the location of each atom by dividing the Coulomb force felt by the atom by the atomic charge. After the initial application of the electric field (occurs over 1 fs), the average x component of the effective electric field rapidly increased until it reached a saturation value (Figure 1a). We have defined the saturation time t_s to be the time required for the effective electric field to reach 95% of its maximum value. The average electric field remained stable with oscillations of at most 5% for $t_p < t < t_{onset}$. The changes in the electric field near the onset of cavitation will be discussed below. The saturation value decreased (Figure 1b), and the pulse time increased exponentially (Figure 1c) as the applied electric field decreased. The time resolution in these calculations is 1 ps. For $\mathbf{E}_{app} > 0.125$ V/Å, a smaller timescale is needed for accurate measurements. The saturation time increases from between 3 and 4 ps for a 0.25 V/Å applied field to 20 ps for the 0.0524 V/Å field. Analysis of the log E versus log t_p of the data in Figure 1 yielded a slope of −0.97, which indicates an exponential dependence. The total electric field increased linearly with the applied electric field; however, there was a scaling factor of approximately 3.6. This increase in total electric field strength is attributed to the polarization of the water molecules and resulting dipole moment of the periodic simulation boxes.[18] The effective electric field for a constant applied electric field is given by

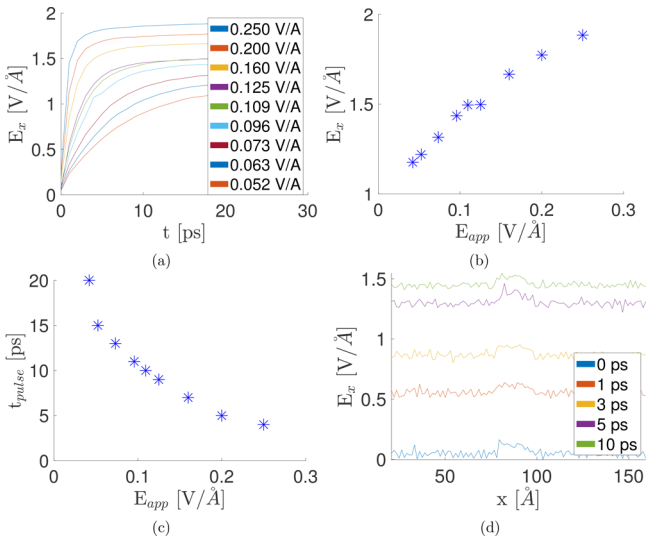

Figure 1. Initial magnitude and structure of electric field. (a) Average x component of the electric field versus time for different applied electric field strengths. (b) Time it takes for the electric field to reach 95% of the saturation value. (c) Magnitude of the saturation value for the electric field versus applied electric field. (d) The x dependence of the x component of the electric field at different time steps corresponds to the initial application of the field, the rise, and the saturation for an applied field of 0.125 V/Å.

$$\mathbf{E}_{eff} = \mathbf{E}_{app} + \mathbf{E}_{dp} \tag{3}$$

where $\mathbf{E}_{dp}$ is the electric field due to the dipole moment of the box

$$\mathbf{E}_{dp} = \frac{\mathbf{p}}{4\pi\epsilon_0}\sum_{\theta,r}\frac{2\cos^2\theta - \sin^2\theta}{r^3} \tag{4}$$

where $\mathbf{p}$ is the total dipole of the box, the sum is over all dipoles within the box, r is the distance from an individual dipole to the position where $\mathbf{E}$ is being measured, and θ is the angle between the dipole and the distance vector between the dipole and measurement point.[19] If we let $\mathbf{p} = \alpha\mathbf{E}_{app}$ where α is the effective polarizability of the box, then the effective electric field becomes

$$\mathbf{E}_{eff} = \mathbf{E}_{app}\left(1 + \frac{\alpha}{4\pi\epsilon_0}\sum_{\theta,r}\frac{2\cos^2\theta - \sin^2\theta}{r^3}\right) \tag{5}$$

Noting that our electric field scales as 3.6 times the applied electric field, the second term in eq 5 must evaluate to 2.6. For steady-state electric fields, the dipole component has been found to be larger than the applied electric field itself, which is in agreement with our results. This would suggest that the dipole relaxation of the water molecules is responsible for the electric field pulses seen in Figure 1a. Figure 1d shows the x component of the electric field at t = 0, 1, 5, and 10 ps for $\mathbf{E}_{app}$ = 0.125 V/Å. From these results, it can be seen that, during this initial pulse, only the magnitude of the electric field changes, while the structure of the electric field does not change. In the absence of a nanoparticle, the pulse occurs on similar timescales (between 3 and 4 ps for 0.25 V/Å); however, cavitation is not observed. This reaffirms that the nanoparticle is required for cavitation in this system. Furthermore, this suggests that alteration of the local electric field is what induces the cavitation.

Figure 2a shows a snapshot of a simulation shortly after cavity genesis. The time of cavitation onset (T_{onset}) was found to relate to the applied electric field through a stretched exponential relaxation response

$$\bar{E} = \exp((t_{onset}/\tau)^{-\beta}) \tag{6}$$

where $\bar{E} = E/E_{max}$ is the electric field divided by the maximum applied electric field (E_{max} = 0.25 V/Å). The value for β was 0.424 ± 0.09 (Figure 2). The value for β was found by plotting log(− log ($\bar{E}$)) versus log T_{onset} and finding the weighted line of best fit (Figure 2b,c). The fitting weights were based on the error associated with each T_{onset} measurement (±1 ps). These values are very close to the "magic" values found in the stretched exponential response theory.

Stretched exponential relaxation has been used to explain relaxation in glasses and dielectrics.[20−22] Across decades of experiments in a wide range of systems, a few magic values for β have arisen. One of the early explanations was the trapping model, in which entropic excitations diffuse freely through the phase space until they reach sinks where they become stuck.[22] The stretched exponential nature then arises as a result of the excitations near the sink being diminished quickly while farther away excitations taking increasing lengths of time due to their distance from the sink. This model predicts a value for β of

DOI: 10.1021/acsomega.9b00979
ACS Omega 2019, 4, 22274−22279

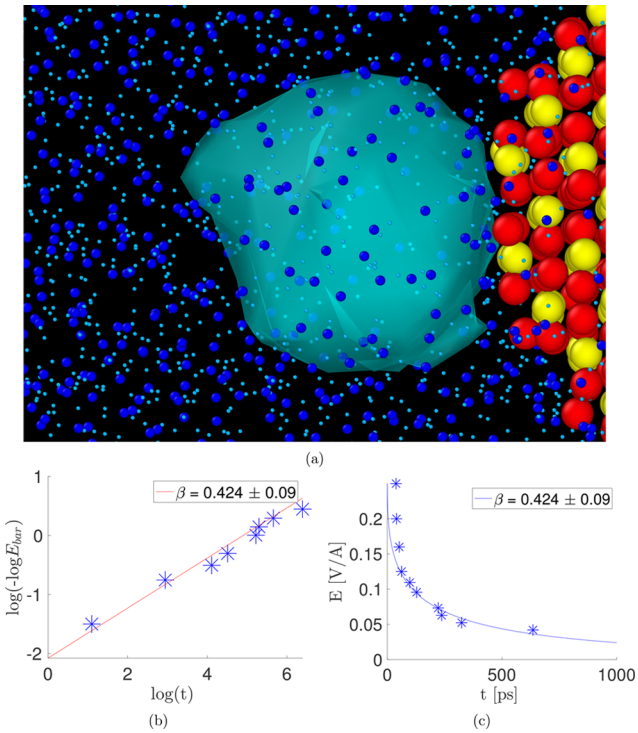

Figure 2. (a) Snapshot of the system just after cavitation. (b) $\overline{E}$ versus t: blue markers are the data used to calculate the exponential relaxation coefficient β. The temporal data span an order of magnitude (60 to 635 ps). The red line is the fitted line of best fit. (c) The blue line is the plotted stretched exponential function with $\beta = 0.424$ and $\tau = 134.6$ ps.

$$\beta = \frac{d}{d+2} \tag{7}$$

where d is the dimensionality of the system. Phillips,[22] using the wealth of experimental data, proposed an axiomatic model with the axiom

$$\beta = \frac{d^*}{d^*+2} = \frac{d}{d+2/f} \tag{8}$$

where $d^* = fd$, and f is the number of short range forces available for relaxation divided by the number of long-ranged forces. A topological justification of this model can be found in ref 23. For a system such as the one studied in this paper with one short-ranged interaction per atom type (Lennard–Jones/Buckingham) and one long-ranged force (the Coulomb force), one would expect $f = 1/2$, yielding $\beta = 3/7$. Further discussion on the interpretation of β can be found in the Supporting Information.

Figure 3a–f shows the evolution of the cavity with respect to time for an applied field of 0.042 V/Å. Snapshots shown are from 500, 650, 750, 850, 1000, and 1100 ps. The cavity volume as a function of time is shown for the duration of the simulation in Figure 3g. Between 500 and 650 ps, the cavity begins to form in front of the nanoparticle. Between approximately 650 and 730 ps, the cavity forms and expands roughly spherically at a rate of approximately 24.7 Å^3/ps. The cavity then expands cylindrically at a rate of 92.78 Å^3/ps for 150 ps. After the initial sphere phase, the cavity grows in a cigar-like fashion: First, a small tendril of the cavity extends in the direction of the electric field, away from the midpoint of the nanoparticle, and then it expands outward until the segment reaches the same cyclindrical radius as the rest of the cavity. The cavity stabilizes for a period of 90 ps until it continues to grow at a reduced rate of 29 Å^3/ps. Between 1050

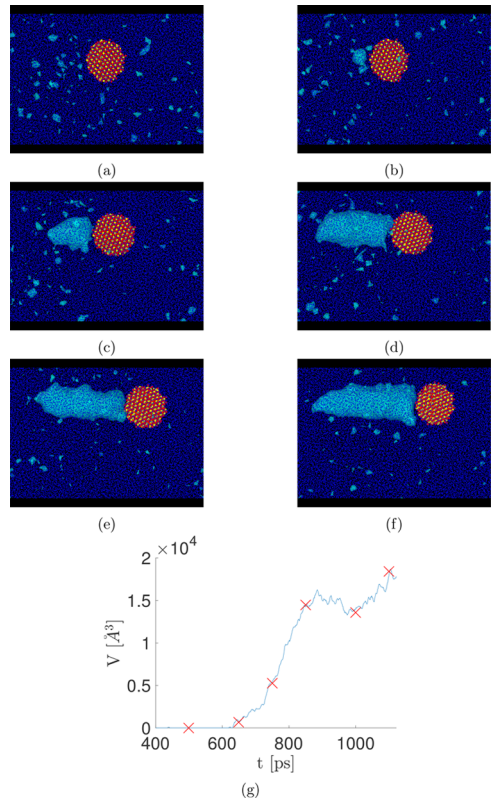

Figure 3. Evolution of cavity with an applied 0.42 V/Å electric field. Snapshots at T = (a) 700, (b) 800, (c) 900, (d) 1000, (e) 1050, and (f) 1100 ps. (g) Cavity volume as a function of time with red X's over the data points corresponding to (a)–(f).

and 1100 ps, the outermost (from the nanoparticle) segment broke off and collapsed. Yet, in that time span, the overall cavity volume continued to expand. During this new regime, the volume increase comes from an expansion in the radial direction.

An explanation for the cylindircal growth of the void cavity is found in the literature.[8] The equation for square magnitude of the electric field near a spherical void is given by

$$E^2(r,\theta) = \mathbf{E}_{\text{app}}{}^2\left(1 + (3\cos^2\theta + 1)\left(\frac{\epsilon - 1}{2\epsilon + 1}\right)^2\frac{R^6}{r^6} - (5\cos^2\theta - 1)\frac{R^3}{r^3}\frac{\epsilon - 1}{2\epsilon + 1}\right) \tag{9}$$

with θ donating the angle between r and the external applied electric field $\mathbf{E}_{\text{app}}$. The volumetric force near the pore ($R < r < 2.5R$) then becomes[8]

$$F \approx \frac{3}{2}\alpha\epsilon_0\epsilon{E_0}^2\frac{(\epsilon - 1)R^3}{(2\epsilon + 1)r^4}\left((5\cos^2\theta - 1) - 2(3\cos^2\theta + 1)\frac{R^3(\epsilon - 1)}{r^3(2\epsilon + 1)}\right)$$

Notice that, when $\theta = 0$, which is in line with the external applied electric field, the electric field is minimized and the force is positive (pointing radially outward). As θ increases, the electric field in this region increases and the force becomes less positive until it becomes negative between $\pi/8$ and $\pi/4$. This would explain the cigar shape found in the simulations.

DOI: 10.1021/acsomega.9b00979
ACS Omega 2019, 4, 22274–22279

There were two apparent growth phases in cavitation genesis: an initial spherical phase and a longer-lasting cylindrical growth phase. From inspection of Figure 4, two distinct growth slopes

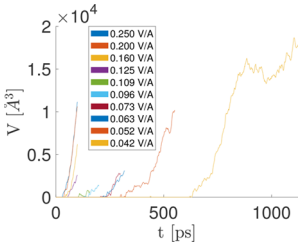

Figure 4. Cavity volume analysis. Cavity volume as a function of time for different applied electric fields. In most of the curves, two distinct regions of near-linear growth appear. The first curve corresponds to the spherical growth phase, while the second one corresponds to the cylindrical growth phase.

emerge. Generally, both phases grew at increased rates as the electric field strength was increased. The volume growth appears to grow linearly; however, the data are too noisy to determine this definitively. A description of how the void volumes were calculated can be found in the Supporting Information.

The x component of the electric field was calcualted by dividing the Coulomb force by atomic charge for each hydrogen and TIP4P dummy atom of water and each tin and oxygen atom corresponding to tin dioxide (Figure 5). The x component of the electric field was averaged and compressed into the y-z plane (Figure 5a,d,g) and along the x axis (Figure 5b,e,f). The snapshots were taken from the $\mathbf{E}_{app}$ = 0.125 V/Å run. The nanoparticle disrupts the otherwise constant electric field, which produces the inhomogeneity required for cavity formation. Once the bubble has formed (t = 100 ps), the average electric field in the water spikes heavily in the plane around the bubble, in agreement with eq 9, while seeing a slighly reduced electric field near the leftmost edge. The internal electric field strength in the absence of an externally applied electric field has been found to be between 1.5 and 2.5 V/Å[24] with only modest alterations due to a comparatively weaker $\mathbf{E}_{app}$. This is in line with the electric field results in Figure 5.

SUMMARY

We have observed cavitation in MD simulations of a SnO_2 nanoparticle immersed in water modeled by SPC/E and the hydrogen bonding polarizable force fields. The results from these simulations describe a general phenomenon. Cavity growth rates indicate spherical and cylindrical growth phases. These growth phases are analyzed as a function of the applied electric field, and the simulation data are consistent with the theoretical calculation for a cigar-shaped cavity near the nanoparticle. A more precise anaylsis of the cavity shape and evolution will be the subject of future work. The cavitation onset time as a function of the applied electric field displays a stretched exponential relaxation response with a universal value for the exponent, $\beta = d^*/(d^* + 2) = 3/7$, for systems with long-ranged forces. Identifying the long timescale value of β provides evidence for the most likely mechanism behind cavitation; that is, the thermally activated cavities diffuse into the main cavity by

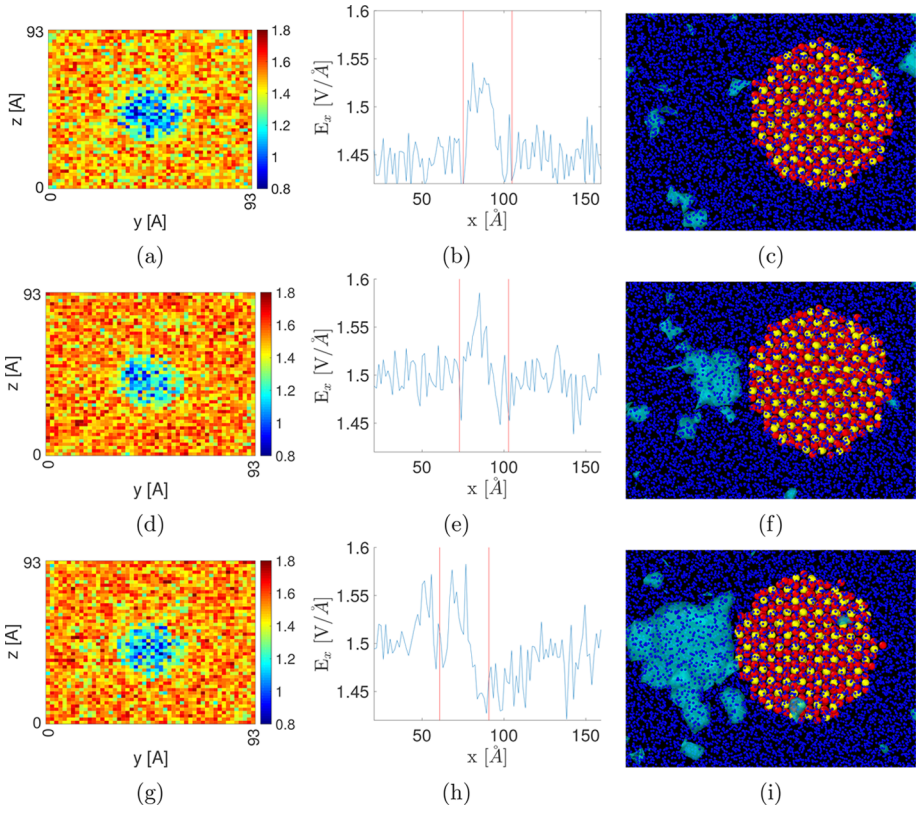

Figure 5. x component of the electric field at (a−c) 10 ps, (d−f) 40 ps, and (g−i) 100 ps for an applied field of 0.125 V/Å. (a, d, g) Heat map of E_x averaged over the x axis. (b, e, h) Plot of E_x versus x position averaged over y and z axes. The red lines show the locations of the edge of the nanoparticle. (c, f, i) Snapshot of the cavity and nanoparticle at a time step under consideration. The electric field spikes in the region around the cavity while decaying as the distance is increased from the cavity.

DOI: 10.1021/acsomega.9b00979
ACS Omega 2019, 4, 22274−22279

the nanoparticle. These results can be verified by creating a solution of tin dioxide nanoparticles suspended in water and creating a sufficiently strong electric field through the use of a fast pump laser and observing cavitation with the free electron laser facility at SLAC National Accelerator Laboratory.[25] The Linac Coherent Light Source (LCLS) at SLAC has been used to successfully study fragile proteins[26] and to investigate femtosecond timescale phenomenon.[27] The same techniques could be used to probe our system. Experimental verification of these simulations will provide an interesting direction for further research.

COMPUTATIONAL METHODS

Cavitation was observed with both SPC water and polarizable water force fields; however, the simulations discussed within this paper were all done with a combination of the SnO_2 force field developed by Bandura et al.[7] with the hydrogen bonding polarizable (HBP) water force field.[28] Further details on the force fields can be found in the Supporting Information.

Bulk crystal SnO_2 was simulated to generate nanoparticles. The equilibrated nanoparticle was then placed into a prepared water box. Finally, the combined system was used to run the electric field simulations described below. All simulations were done using LAMMPS. The default velocity Verlet integrator was used with a time step of 1 fs. Periodic boundary conditions were used in every simulation.

The 199,970-atom combined water and nanoparticle system was used at the starting point for the simulations described in this paper. Simulations ran from 100 ps to 1.2 ns. Uniform electric fields ranging from 0.042 to 0.25 V/Å were applied along the x direction. Electric field strengths above 0.25 V/Å were ignored because force fields that can deal with bond breaking such as ReaxFF are required as water will dissociate at such high field strengths. The Ewald summation method was used with tin-foil boundary conditions to calculate the Coulomb force with a maximum relative error in the forces of 1.0×10^{-5}.

ASSOCIATED CONTENT

Supporting Information

The Supporting Information is available free of charge at https://pubs.acs.org/doi/10.1021/acsomega.9b00979.

Detailed description of force fields used, description of water only simulations, description of void volume calculation methods, and further discussion on β (PDF)

Movie of the 0.629 V/Å simulation showing the formation of the cavity (MOV)

AUTHOR INFORMATION

Corresponding Authors

*E-mail: swjackso@usc.edu (S.J.).
*E-mail: anakano@usc.edu (A.N.).
*E-mail: priyav@usc.edu (P.V.).
*E-mail: rkalia@usc.edu (R.K.K.).

ORCID

Shane Jackson: 0000-0002-2663-8235
Priya Vashishta: 0000-0003-4683-429X

Notes

The authors declare no competing financial interest.

ACKNOWLEDGMENTS

This work was supported by the U.S. Department of Energy, Office of Science, Basic Energy Sciences, Materials Science and Engineering Division, grant DE-SC0018195. This work was performed, in part, at the Center for Integrated Nanotechnologies, an Office of Science User Facility operated for the U.S. Department of Energy (DOE) Office of Science. Sandia National Laboratories is a multimission laboratory managed and operated by National Technology and Engineering Solutions of Sandia, LLC, a wholly owned subsidiary of Honeywell International, Inc., for the U.S. DOE's National Nuclear Security Administration under contract DE-NA-0003525. The views expressed in the article do not necessarily represent the views of the U.S. DOE or the U.S. Government. We would like to thank M. Winterer for his aid in developing an experiment proposal.

REFERENCES

(1) Agarwal, A.; Ng, W. J.; Liu, Y. Principle and applications of microbubble and nanobubble technology for water treatment. *Chemosphere* **2011**, *84*, 1175−1180.
(2) Torchilin, V. P. Recent advances with liposomes as pharmaceutical carriers. *Nat. Rev. Drug Discovery* **2005**, *4*, 145.
(3) Nomura, K.; Kalia, R. K.; Nakano, A.; Vashishta, P.; van Duin, A. C. T. Mechanochemistry of shock-induced nanobubble collapse near silica in water. *Appl. Phys. Lett.* **2012**, *101*, No. 073108.
(4) Weninger, K. R.; Camara, C. G.; Putterman, S. J. Observation of bubble dynamics within luminescent cavitation clouds: Sonoluminescence at the nano-scale. *Phys. Rev. E* **2000**, *63*, No. 016310.
(5) Azouzi, M. E. M.; Ramboz, C.; Lenain, J.-F.; Caupin, F. A coherent picture of water at extreme negative pressure. *Nat. Phys.* **2013**, *9*, 38.
(6) Shneider, M.; Pekker, M. Cavitation in dielectric fluid in inhomogeneous pulsed electric field. *J. Appl. Phys.* **2013**, *114*, 214906.
(7) Bandura, A. V.; Sofo, J. O.; Kubicki, J. D. Derivation of force field parameters for SnO_2- H_2O surface systems from plane-wave density functional theory calculations. *J. Phys. Chem. B* **2006**, *110*, 8386−8397.
(8) Shneider, M. N.; Pekker, M. Pre-breakdown processes in a dielectric fluid in inhomogeneous pulsed electric fields. *J. Appl. Phys.* **2015**, *117*, 224902.
(9) Caupin, F.; Herbert, E. Cavitation in water: a review. *C. R. Phys.* **2006**, *7*, 1000−1017.
(10) Zheng, Q.; Durben, D. J.; Wolf, G. H.; Angell, C. A. Liquids at large negative pressures: water at the homogeneous nucleation limit. *Science* **1991**, *254*, 829−832.
(11) Green, J. L.; Durben, D. J.; Wolf, G. H.; Angell, C. A. Water and solutions at negative pressure: Raman spectroscopic study to-80 Megapascals. *Science* **1990**, *249*, 649−652.
(12) Shneider, M. N.; Pekker, M. Rayleigh scattering on the cavitation region emerging in liquids. *Opt. Lett.* **2016**, *41*, 1090−1093.
(13) Seepersad, Y.; Fridman, A.; Dobrynin, D. Anode initiated impulse breakdown in water: the dependence on pulse rise time for nanosecond and sub-nanosecond pulses and initiation mechanism based on electrostriction. *J. Phys. D: Appl. Phys.* **2015**, *48*, 424012.
(14) Plimpton, S. Fast parallel algorithms for short-range molecular dynamics. *J. Comput. Phys.* **1995**, *117*, 1−19.
(15) Thompson, A. P.; Plimpton, S. J.; Mattson, W. General formulation of pressure and stress tensor for arbitrary many-body interaction potentials under periodic boundary conditions. *J. Chem Phys.* **2009**, *131*, 154107.
(16) Sirk, T. W.; Moore, S.; Brown, E. F. Characteristics of thermal conductivity in classical water models. *J. Chem. Phys.* **2013**, *138*, No. 064505.
(17) Scovell, D. L.; Pinkerton, T. D.; Medvedev, V. K.; Stuve, E. M. Phase transitions in vapor-deposited water under the influence of high surface electric fields. *Surf. Sci.* **2000**, *457*, 365−376.
(18) Caleman, C.; Van Der Spoel, D. Picosecond melting of ice by an infrared laser pulse: A simulation study. *Angew. Chem., Int. Ed.* **2008**, *47*, 1417−1420.

DOI: 10.1021/acsomega.9b00979
ACS Omega 2019, 4, 22274−22279

(19) English, N. J.; Waldron, C. J. Perspectives on external electric fields in molecular simulation: progress, prospects and challenges. *Phys. Chem. Chem. Phys.* **2015**, *17*, 12407−12440.
(20) Phillips, J. C. Stretched exponential relaxation in molecular and electronic glasses. *Rep. Prog. Phys.* **1996**, *59*, 1133.
(21) Potuzak, M.; Welch, R. C.; Mauro, J. C. Topological origin of stretched exponential relaxation in glass. *J. Chem. Phys.* **2011**, *135*, 214502.
(22) Phillips, J. C. Axiomatic theories of ideal stretched exponential relaxation (SER). *J. Non-Cryst. Solids* **2006**, *352*, 4490−4494.
(23) Macdonald, J. R.; Phillips, J. C. Topological derivation of shape exponents for stretched exponential relaxation. *J. Chem. Phys.* **2005**, *122*, No. 074510.
(24) English, N. J.; MacElroy, J. M. D. Hydrogen bonding and molecular mobility in liquid water in external electromagnetic fields. *J. Chem. Phys.* **2003**, *119*, 11806−11813.
(25) Winterer, M. Personal communication, University of Duisburg, 2019.
(26) Kern, J.; Alonso-Mori, R.; Tran, R.; Hattne, J.; Gildea, R. J.; Echols, N.; Glöckner, C.; Hellmich, J.; Laksmono, H.; Sierra, R. G.; et al. Simultaneous femtosecond X-ray spectroscopy and diffraction of photosystem II at room temperature. *Science* **2013**, *340*, 491−495.
(27) Sierra, R. G.; Laksmono, H.; Kern, J.; Tran, R.; Hattne, J.; Alonso-Mori, R.; Lassalle-Kaiser, B.; Glöckner, C.; Hellmich, J.; Schafer, D. W.; et al. Nanoflow electrospinning serial femtosecond crystallography. *Acta Crystallogr., Sect. D: Biol. Crystallogr.* **2012**, *68*, 1584−1587.
(28) Jiang, H.; Moultos, O. A.; Economou, I. G.; Panagiotopoulos, A. Z. Hydrogen-bonding polarizable intermolecular potential model for water. *J. Phys. Chem. B* **2016**, *120*, 12358−12370.

DOI: 10.1021/acsomega.9b00979
ACS Omega 2019, 4, 22274−22279